Short-Wave Infrared Sensor by the Photothermal Effect of Colloidal Gold Nanorods

Hengyang Xiang, Tingting Niu, Mathilde Schoenauer Sebag, Zhelu Hu, Xiangzhen Xu, Laurent Billot, Lionel Aigouy, Zhuoying Chen

Short-Wave Infrared Sensor by the Photothermal Effect of Colloidal Gold Nanorods

Hengyang Xiang, Tingting Niu, Mathilde Schoenauer Sebag, Zhelu Hu, Xiangzhen Xu, Laurent Billot, Lionel Aigouy and Zhuoying Chen[*]

H. Xiang, T. Niu, M. Schoenauer Sebag, Z. Hu, Dr. X. Xu, Dr. L. Billot, Dr. L. Aigouy and Dr. Z. Chen
LPEM, ESPCI Paris, PSL Research University, Sorbonne Universités, UPMC, CNRS, 10 Rue Vauquelin, F-75005 Paris, France
[*] E-mail: zhuoying.chen@espci.fr

Keywords: gold nanoparticles, photothermal effect, short-wave infrared, photodetection

Abstract. Photodetection in the short-wave infrared (SWIR) spectrum is a challenging task achieved often by costly low-bandgap compound semiconductors involving highly toxic elements. In this work, we report an alternative low-cost approach for SWIR sensors which relies on the plasmonic-induced photothermal effect of solution-processed colloidal gold nanorods (Au NRs). A series of uniform solution-processed Au NRs of various aspect-ratios were prepared exhibiting a strong and well-defined longitudinal LSPR maximum from 900 nm to 1.3 μm. A hybrid device structure was fabricated by applying Au NRs on the surface of a thermistor. Under a monochromatic illumination, hybrid Au-NR/thermistor devices exhibit a clear photoresponse in the form of photo-induced resistance drop in the wavelength window from 1.0 μm to 1.8 μm. The photo-responsivity of such hybrid devices reaches a maximum value of 4.44×10^7 Ω/W at $\lambda = 1.4$ μm (intensity = 0.28 mW/cm^2), a wavelength in agreement with the longitudinal LSPR of the Au NRs applied. Colloidal Au NRs, capable to perform fast conversion between photon absorption and thermal energy, thus open an interesting avenue for alternative low-cost SWIR photodetection.

1. Introduction

Short-wave infrared (SWIR) typically refers to the photons in the wavelength range from 1 to 3 microns. Applications in this wavelength window exploit various advantages such as long penetration length in biological tissue, spectral coverage of the atmospheric nightglow, and the characteristic excitation energy of certain molecular vibration modes.[1–3] SWIR photodetectors are thus the key technological components to achieve optical communication, environmental gas sensing, biodiagnostics and passive night vision.[4] Current SWIR technologies mainly rely on low-bandgap compound semiconductors such as InGaAs, InSb, PbS and HgCdTe. While classical SWIR photodetectors exhibit excellent detectivity, they are costly (due to epitaxial growth requirement) and/or environment unfriendly involving highly toxic elements. There are therefore continuous research and development efforts for alternative material systems and fabrication methods to expand the scope of applications of SWIR photodetection.

For example, graphene is an emerging two-dimensional material candidate allowing broadband and ultrafast photodetection.[5–7] Colloidal semiconducting nanocrystals such as PbS are also excellent material choices towards low-cost SWIR photodetection.[8] Hybrid devices, taking advantage of both the high carrier mobility of two-dimensional materials and the large absorption cross-section of colloidal nanocrystals, are also highly promissing.[9–11] Finally, besides the above-mentioned semiconducting materials, plasmonic nanostructures based on noble metal represent another class of new materials to enable SWIR photodetection.[12] Current plasmonic photodetectors rely on the extraction of “hot carriers” (*i.e.* highly energetic carriers not in thermal equilibrium with the metal atoms) produced during the decay of the localized surface plasmons from a metal nanostructure. Based on this principle various hot-carrier photodetectors were fabricated by lithographically defined nanostructures exhibiting photoresponsivity ranging from a few nA/W to a few tens of mA/W.[13–15]

In this work, we report an alternative approach for SWIR sensors which relies on the plasmonic-induced photothermal effect of solution-processed colloidal gold nanorods. Noble metal nanoparticles have a large optical absorption cross-section for photons in the wavelength range corresponding to their localized surface plasmon resonance (LSPR).[16] Following photon absorption and subsequent LSPR excitation in a metal nanoparticle, plasmon resonance decays either radiatively by re-emitting a photon or non-radiatively through Landau damping generating hot carriers on a time scale ranging from 1 to 100 fs after LSPR excitation.[17] Hot carriers, if not extracted through a specific device structure, will then quickly redistribute their energy towards lower energy electrons via electron-electron scattering followed by thermalisation with the lattice and heat transferred to the surroundings on a time scale ranging from 100 ps to 10 ns. Metal nanoparticles are therefore efficient mediums to convert photons to thermal energy. The remarkable photothermal effect of metal nanoparticles has since been applied in many fields such as catalysis,[18,19] solar energy harvest,[20,21] optical switching,[22] cancer therapy,[23–26] and drug delivery.[27] Yet this effect has not been explored on SWIR photodetection. The LSPR wavelength of metal nanoparticles can be readily tuned by controlling the nanoparticle composition, dimension, shape and the surrounding dielectric environment.[28,29] Among different plasmonic nanoparticles, gold nanorods exhibit distinctive longitudinal and transverse LSPR owing to their anisotropic shape. In particular, their longitudinal LSPR position is tunable from the visible to the near-infrared spectrum by controlling their aspect ratio from colloidal synthesis.[30–32] While most current applications of the photothermal effect of gold nanorods concerns the spectrum range from the visible to near-infrared, examples exploiting the wavelength range > 1 μm are still rare.

Here, by a careful synthetic tuning, we obtained a series of monodisperse colloidal gold nanorods of different aspect ratios with their longitudinal LSPR maximum tunable from 900 nm to 1.3 μm. Applying these solution-processed nanorods into a hybrid device structure in

combination with a thermistor, we observed clear photoresponsivity in the spectrum range from 1.0 μm to 1.8 μm. After examining the photoresponse characteristics, we revealed that the response-speed limitation of the hybrid device origins from the thermistor but not from the gold nanorods. Colloidal gold nanorods, capable to perform fast conversion between photon absorption and thermal energy, thus open an interesting avenue for alternative low-cost SWIR photodetection.

2. Results and Discussion

A series of monodisperse colloidal gold nanorods (Au NRs) of different aspect ratios (ARs) were synthesized by modifying the silver-assisted seed-mediated growth method applying binary surfactants reported previously.[31] While most reported colloidal Au NRs exhibit a longitudinal LSPR (L-LSPR) in the wavelength range shorter than 1200 nm,[30,31,33–35] we successfully extend the aspect ratio (AR) of Au NRs up to 10.96 with their L-LSPR absorption peak reaching 1300 nm. Such a synthesis involved first the formation of gold nanoparticle seeds by reducing gold(III) chloride ($HAuCl_4$) by sodium borohydride ($NaBH_4$) in the presence of hexadecyltrimethylammonium bromide (CTAB) as surfactant. Different amounts of Au seeds were further placed into a growth solution where Au(III) is slowly reduced by a combination of ascorbic acid (AA) and sodium oleate (NaOL) in the presence of hydrochloric acid (HCl), CTAB and silver nitrate ($AgNO_3$) (detailed procedure described in the experimental section). In such a multi-parameter synthesis, we have specifically experimented various amounts of Au seeds, $AgNO_3$, surfactant NaOL, and the acidity of the growth solution (amounts of HCl) (summarized in **Table 1**). Comparing the results of sample c and sample e (table 1), we observed an increased average length and diameter of Au NRs associated with the decreased amount of Au seeds, which is possibly due to more growth material available per seed. Sample e exhibited a larger AR compared to sample c due to their smaller NR width (diameter). The role of Ag^{3+} in such a synthesis has been reported as crucial

as it interacts with CTAB to form elongated templates and hinders the growth of certain crystallographic facets of Au NRs.[36,37] Increasing the amount of Ag^{3+} from the optimum value however led to a decrease of AR due to the thickened NR width (comparing sample b and c, table1). Concerning the amount of surfactant NaOL, we observed longer and thicker Au NRs with larger AR when the amount of NaOL decreases from 1.234 g to 0.925 g (sample f and g, table 1). The use of NaOL here together with CTAB in the growth solution represents a binary surfactant strategy. NaOL serves here both as a reduction agent and likely also as a surface binding mediator between CTAB and certain facet of Au to allow NR morphological tuning.[31] Concerning HCl, one modifies the NR growth by controlling the acidity of the growth solution. A larger amount of HCl here led to a reduction of pH favoring larger AR by reducing more significantly the width of NRs (sample g and h, table 1). By controlling these four parameters we were able to tune the AR of NRs from 4.47 to 10.96. As the L-LSPR of Au NRs are highly sensitive to their AR, this series of samples thus exhibits distinctive optical property with a strong and well-defined L-LSPR progressively red-shifted towards 1300 nm as AR increases (**Figure 1**). The evolution of the L-LSPR maximum over the AR of NRs roughly follows a linear relation (Figure 1f). The asymmetric shape of the L-LSPR absorbance of samples g and h (table 1, and the green and red curve of Figure 1e) are formed due to the artifact originated from water absorption. This artifact disappeared in the UV-Vis absorbance when samples are in a form of solid thin films (supporting information **Figure S1**). The small contribution of the transverse-LSPR lies in the wavelength range between 650 to 700 nm, which is relatively less sensitive to the change of AR compared to L-LSPR. The absorption contribution at about 525 nm originates from the existence of semi-spherical Au nanoparticles, which are impurities in the Au NR synthesis. While the proportion of these impurities over Au NRs slightly increased in a NR synthesis for high AR, the majority of the synthetic products of the whole series of samples remained to be NRs of high uniformity as shown in transmission electron microscopy (TEM) characterization (Figure 1 and **Figure S2**

in the supporting information). The minor contribution of these synthetic impurities (semi-spherical Au nanoparticles) to the hybrid device characteristics was described in the supporting information.

To harvest the remarkable photothermal effect of Au NRs, as a proof-of-concept we applied a low-cost negative temperature coefficient (NTC) thermistor with a room-temperature (25 °C) resistance of 10 kΩ (Series B57540G1 from TDK EPCOS) for the fabrication of hybrid devices: 1 drop (~ 3 μL) of as-synthesized Au NRs in water with a concentration ranging from 0.6 g/L to 7.2 g/L was drop-casted directly to coat the thermistor surface leading to the formation of a hybrid Au-NR/thermistor device (**Figure 2**). In order to perform sensing in the SWIR spectrum, we selected the sample h of table 1 with a L-LSPR maximum at 1300 nm to fabricate such Au-NR/thermistor hybrid devices. Data of Au-NR/thermistor hybrid devices based on another batch of NR sample (sample b of table 1) was shown in the supporting information. Scanning electron microscopy (SEM) characterization, carried out directly on an Au NR-coated thermistor, confirmed the thermistor surface coating to be dominated by Au NRs (Figure 2d). With Au NR solution of a higher concentration dense random packing of Au NRs were observed (supporting information **Figure S3**). In such a hybrid configuration, Au NRs serve as the photon absorption agent and generate heat as a result of the decay of LSPR excitation. The generated heat leads to a *drop* of the resistance of the NTC thermistor which is in contact with Au NRs and the variation of resistance can be probed by simple electrical measurements (Figure 2e).

We then applied a series of monochromatic illumination ranging from 1.0 μm to 1.8 μm and we studied the photoresponse of the hybrid Au-NR/thermistor (**Figure 3**). This series of monochromatic illumination were generated by a quartz halogen lamp, a monochromator and relevant filters. The density of illumination, determined by the lamp and the grating of the monochromator, was calibrated to be from 0.16 mW/cm^2 (at 1800 nm) to 0.35 mW/cm^2 (at

1300 nm). Under each monochromatic illumination, a "control device" containing only the thermistor (without Au NRs) was equally experimented and we observed limited photoresponse at the whole wavelength range (grey curves of Figure 3a). In these experiments, the illumination applied is of relatively low intensity and therefore negligible photo-induced heating effect were observed on the control device. By comparison, under the same illumination condition, hybrid Au-NR/thermistor exhibited a clear photoresponse revealed by a photo-induced resistance drop (Figure 3a). Here the existence of Au NRs on the surface of the thermistor and their photothermal effect enable a measurable photoresponse in the hybrid device in a form of resistance variation. The response time of the hybrid device can be characterized by the rise and decay time, respectively defined here as the time used by the resistance to drop from its room-temperature value to 70% of the saturation level (when illumination is on) and the time used by the resistance to increase back to 70% of its room-temperature value (when illumination is off). As shown in Figure 3b, both the rise and decay time of the hybrid device are less than a few seconds. After normalizing the photo-induced resistance drop by the intensity of the illumination, we obtained the responsivity (in Ω/W) of the hybrid device over the whole wavelength window tested. From the datasheet of the thermistor we obtained the corresponding responsivity in °C /W. As shown in Figure 3c, in the wavelength window experimented, the maximum photo-responsivity of hybrid Au-NR/thermistor devices shifted slightly from λ = 1.3 μm to 1.4 μm when a more concentrated Au NR solution was applied. For devices fabricated by relatively diluted Au NR solutions (e.g. 0.6 g/L and 1.2 g/L), the responsivity peak wavelength is in good agreement with the L-LSPR maximum of the Au NRs applied. For devices fabricated by a more concentrated Au NR solution (4.8 g/L), the dense packing of Au NRs may lead to the observed red-shift of the responsivity maximum. Besides the slight red-shifting of the responsivity maximum, the responsivity magnitude of the hybrid devices increased as the Au NR solution concentration increased from 0.6 g/L to 4.8 g/L. This is coherent with the fact that more Au NRs are

available on the thermistor surface to exercise their nano-heater function when a more concentration Au NR solution was applied. With a further increased concentration (> 4.8 g/L), however, we started to observe a decrease of hybrid device performance (supporting information Figure S4), likely due to the increased limitation of heat-transfer from very dense Au NRs clusters to the thermistor. The most optimized hybrid device, fabricated by 4.8 g/L Au NR solution, exhibited a maximum photo-responsivity of 4.44×10^7 Ω/W at λ = 1.4 μm (0.28 mW/cm^2).

In order to understand the process which limits the response speed of this type of hybrid Au-NR/thermistor, on the most optimized hybrid device fabricated by 4.8 g/L Au NR solution we further studied their photoresponse characteristics under larger illumination intensities (by a laser diode illumination at λ = 1.5 μm). In these experiments a laser spot was focused onto the surface of the hybrid device. Various laser powers ranging from 75 μW to 50 mW were experimented (which corresponds to a power densities ranging from 6.7 mW/cm^2 to 4464.3 mW/cm^2). In this case, as the illumination intensity is relatively high, on a control device (thermistor without Au NRs) we can already observe a response due to the laser-induced heating detected by the thermistor (curves with empty symbols in **Figure 4a**). By comparison, the existence of Au NRs on the surface of hybrid Au-NR/thermistor devices enable a clear enhancement of photoresponse (curves with solid symbols in Figure 4a and Figure S7). After normalizing the response characteristics of the control device and the hybrid device, near-identical rise and fall time, on the scale of 2 s, were observed on both devices (Figure 4b). This suggests that the limitation of response speed of the optimized hybrid device does not originate from the photothermal effect of Au NRs nor from the heat-transfer processes between the Au NRs and the thermistor. Instead, the limitation of response speed comes from the response speed of the thermistor itself. This suggests that the hybrid Au-NR/thermistor device can potentially exhibit a shorter response time if a more performing thermistor is

applied in the hybrid device structure. The photoresponsivity (in °C/W) of both the control and the hybrid device at each experimented laser intensity were shown in Figure 4c. In particular, the hybrid device exhibited a remarkable responsivity enhancement compared to the control device for up to *5.19-fold* enhancement at 0.5 mW laser illumination. For both control and hybrid devices the photoresponsivity decreases as the laser power increases. From previous studies,[38,39] we do not expect the absorption of Au NRs saturates at the current laser intensity window. After extracting the enhancement ratio from the responsivity of the hybrid over the control device (Figure 4d), one observed that the enhancement ratios are roughly of the same order of magnitude over the whole laser power window experimented. This suggests that the decrease of responsivity along with increasing laser power originates again from the thermistor itself. Au NRs here in the hybrid device serve as a sensitizing agent either enabling SWIR photodetection when the illumination intensity is low ($\leq$ 0.35 mW/cm^2, the case shown in Figure 3) or boost the photoresponsivity when the illumination intensity is high (the case of shown in Figure 4). From the data sheet of the thermistor it is possible to obtain the magnitude of photo-induced temperature change corresponding to the resistance change under each laser power experimented (Figure 5). By subtracting the temperature change observed in the control device from that of the hybrid device, we estimated that the laser-induced temperature increase contributed from the Au NRs can be as high as 66 °C at a laser power of 50 mW (λ = 1.5 μm).

3. Conclusion

Started from colloidal synthesis, we prepared a series of uniform solution-processed Au NRs of various ARs (aspect-ratios) exhibiting a strong and well-defined L-LSPR maximum from 900 nm to 1.3 μm. A hybrid device structure, composing of Au NRs on the surface of a NTC-thermistor, was proposed as an alternative low-cost approach for sensing in the SWIR

spectrum. Under a monochromatic illumination of relatively low intensity (≤ 0.35 mW/cm^2), hybrid Au-NR/thermistor devices exhibited a clear photoresponse in the form of photo-induced resistance drop in the wavelength window from 1.0 μm to 1.8 μm. This was in contrast to the control device (thermistor alone without Au NRs), the photoresponse of which was negligible under the same illumination condition. The photo-responsivity of the optimized hybrid device reached a maximum value of 4.44×10^7 Ω/W at 1.4 μm, a wavelength in agreement with the L-LSPR of the Au NRs applied. At higher illumination intensities (from 6.7 mW/cm^2 to 4464.3 mW/cm^2) achieved by a laser (λ = 1.5 μm) focused onto device, due to the laser-induced heating, photoresponse was observed in both the control and the hybrid device. Nevertheless, in this case hybrid devices exhibited more than 5-fold enhancement of photoresponsivity by comparison to the control device.

In summary, the plasmonic-induced photothermal effect of Au NRs (i) enables the photo-sensing capability in a hybrid Au-NR/thermistor device structure under relatively weak illumination and (ii) boosts the photo-response of the hybrid device when illumination intensity is high. The response speed of the current Au-NR/thermistor hybrid device is as short as 2 seconds, limited by the response speed of the thermistor itself. Optical sensing in the SWIR spectrum is a challenging task, the current approach harvesting the photothermal effect of solution-processed colloidal Au NRs thus represent a new path towards alternative and low-cost SWIR sensing.

4. Experimental Section

Synthesis colloidal Au nanoparticle seed solution: After mixing 5 ml of 0.5 mM $HAuCl_4$ solution with 5 ml of 0.2 M CTAB solution, 1 ml of 0.006 M $NaBH_4$ solution was added followed by vigorously stirring for 2 minutes. This solution was then left un-stirred for aging during 30 minutes.

Preparation of Au NR growth solution: 9 g of CTAB was evenly mixed with different amounts of NaOL (listed in table 1). They are then dissolved in 250 ml of de-ionized water under stirring at 50 °C. After the solution was cooled down to 30 °C, different amounts of 4.15 mM $AgNO_3$ solution were added and the whole solution was kept at 30 °C for 15 minutes. This is followed by the addition of 250 ml of 1 mM $HAuCl_4$ solution under stirring for about 90 minutes (until the solution turned colourless). At this stage, different amounts of a 12.1 M HCl solution were added under stirring for 15 minutes. 1.25ml of 0.064 M ascorbic acid solution was then added under vigorous stirring for 30s. Finally, different volumes of Au seed solution prepared above were added first under rigorous stirring for 30s then the whole solution was kept un-stirred for 12 hours at 30 °C for NR growth. Different synthetic parameters are summarized in table 1. After 12 hours of growth the final product was isolated by centrifugation (6k rpm for 30 minutes) and subsequent decantation of mother liquid. De-ionized water was then added to re-dissolved the Au NRs. The centrifugation/decantation process was repeated for 3 times and the final Au NR products were dissolved in de-ionized water.

Nanoparticle characterization: UV-Visible absorption spectra were measured in air using by an Agilent Cary 5E UV-Visible-NIR spectrometer. TEM characterizations were performed by a JEOL 2010 microscope operated at 200 kV. SEM characterizations were performed with a FEI Magellan 400 system with a standard field emission gun source.

Fabrication and characterization of hybrid Au-NR/thermistor devices: A negative temperature coefficient (NTC) thermistor with a room-temperature (25 °C) resistance of 10 kΩ (Series B57540G1103F000 from TDK EPCOS) was obtained from RS components (no. 769-1892, ~ 3 €/each). It is then fixed on a glass microscopy slide. To fabricate the hybrid Au-NR/thermistor device, a drop (~ 3 µL) of Au NR water solution (with a concentration ranging from 0.6 g/L to 7.2 g/L) was casted directly to coat the surface of the thermistor. Hybrid

devices described in the main text were fabricated by the sample h listed in table 1. Data for hybrid devices fabricated by the sample b of table 1 were described in the supporting information. After the Au NR solution was dried on the thermistor, SEM characterizations were performed either directly onto the hybrid device (FEI Magellan 400 system, field emission gun source) or on Au NR-coated glass substrates. The hybrid device was measured under monochromatic illumination generated by a quartz halogen lamp and a computer-controlled Oriel Cornerstone monochromator (and appropriate order sorting filters). The intensity of the monochromatic illumination was calibrated by a NIST-calibrated germanium photodiode. The monochromatic illumination was modulated by a shutter while we measured the resistance of the hybrid and control device by a computer-controlled Keithley 2634B source measurement unit (SMU). Concerning measurements under laser, the output of a fiber-coupled laser diode (λ = 1.5 μm) was focused onto the hybrid or control device. Neutral density filters were used to adjust the laser power while the laser power was calibrated by a laser power meter. The laser illumination was modulated by a shutter while we measured the device resistance by a Keithley 2634B SMU. From the data sheet of the thermistor each resistance value measured corresponds to a temperature point. Therefore, when the illumination was on (or off), we can measure a resistance value of $R_{light\text{-}on}$ (or $R_{light\text{-}off}$). From $R_{light\text{-}on}$ (or $R_{light\text{-}off}$) and the datasheet we obtained the temperature value ($T_{light\text{-}on}$ or $T_{light\text{-}off}$) corresponding to the resistance value measured. From $T_{light\text{-}on}$ and $T_{light\text{-}off}$ we obtained the temperature change ($T_{light\text{-}on}$ - $T_{light\text{-}off}$) of the hybrid device due to the illumination.

Supporting Information

Supporting Information is available from the Wiley Online Library or from the author.

Acknowledgements

This work was supported in part by the UPNAN project (in the framework of IDEX with the reference of ANR-10-IDEX-0001-02 PSL*). SEM characterizations performed were supported by the region Île-de-France in the framework of DIM Nano-K. H. Xiang

acknowledges the China scholarship council (CSC) for PhD thesis scholarship. H. Xiang and T. Niu contributed equally to this work.

Received: ((will be filled in by the editorial staff))
Revised: ((will be filled in by the editorial staff))
Published online: ((will be filled in by the editorial staff))

References

[1] M. Sicard, K. J. Thome, B. G. Crowther, M. W. Smith, *J. Atmos. Ocean. Technol.* **1998**, *15*, 174.
[2] J. Vidot, J. Landgraf, O. P. Hasekamp, A. Butz, A. Galli, P. Tol, I. Aben, *Remote Sens. Environ.* **2012**, *120*, 255.
[3] G. Hong, A. L. Antaris, H. Dai, *Nat. Biomed. Eng.* **2017**, *1*, 10.
[4] M. P. Hansen, D. S. Malchow, *Proc. SPIEE* **2008**, *6939*, 69390I.
[5] C.-H. Liu, Y.-C. Chang, T. B. Norris, Z. Zhong, *Nat. Nanotechnol.* **2014**, *9*, 273.
[6] A. Pospischil, M. Humer, M. M. Furchi, D. Bachmann, R. Guider, T. Fromherz, T. Mueller, *Nat. Photonics* **2013**, *7*, 892.
[7] F. Xia, T. Mueller, Y. Lin, A. Valdes-Garcia, P. Avouris, *Nat. Nanotechnol.* **2009**, *4*, 839.
[8] R. Saran, R. J. Curry, *Nat. Photonics* **2016**, *10*, 81.
[9] Z. Sun, Z. Liu, J. Li, G. A. Tai, S. P. Lau, F. Yan, *Adv. Mater.* **2012**, *24*, 5878.
[10] G. Konstantatos, M. Badioli, L. Gaudreau, J. Osmond, M. Bernechea, F. P. G. de Arquer, F. Gatti, F. H. L. Koppens, *Nat. Nanotechnol.* **2012**, *7*, 363.
[11] Z. Sun, L. Aigouy, Z. Chen, *Nanoscale* **2016**, *8*, 7377.
[12] C. Clavero, *Nat. Photonics* **2014**, *8*, 95.
[13] F. P. García de Arquer, A. Mihi, G. Konstantatos, *ACS Photonics* **2015**, *2*, 950.
[14] H. Chalabi, D. Schoen, M. L. Brongersma, *Nano Lett.* **2014**, *14*, 1374.
[15] A. Sobhani, M. W. Knight, Y. Wang, B. Zheng, N. S. King, L. V. Brown, Z. Fang, P. Nordlander, N. J. Halas, *Nat. Commun.* **2013**, *4*, 1643.
[16] P. Yang, J. Zheng, Y. Xu, Q. Zhang, L. Jiang, *Adv. Mater.* **2016**, *28*, 10508.
[17] M. L. Brongersma, N. J. Halas, P. Nordlander, *Nat. Nanotechnol.* **2015**, *10*, 25.
[18] P. Christopher, H. Xin, S. Linic, *Nat. Chem.* **2011**, *3*, 467.
[19] L. Cao, D. N. Barsic, A. R. Guichard, M. L. Brongersma, *Nano Lett.* **2007**, *7*, 3523.
[20] F. Wang, C. Li, H. Chen, R. Jiang, D. Sun, Q. Li, J. Wang, J. C. Yu, C. Yan, L. Sun, *J. Am. Chem. Soc.* **2013**, *135*, 5588.
[21] Y. Xiong, R. Long, D. Liu, X. Zhong, C. Wang, Z.-Y. Li, Y. Xie, *Nanoscale* **2012**, *4*, 4416.
[22] M. T. Quint, S. Delgado, J. H. Paredes, Z. S. Nuno, S. Linda, S. Ghosh, *Opt. Express* **2015**, *23*, 281.
[23] A. Espinosa, M. Bugnet, G. Radtke, S. Neveu, G. A. Botton, C. Wilhelm, A. Abou-Hassan, *Nanoscale* **2015**, *7*, 18872.
[24] D. Jaque, L. Martínez Maestro, B. del Rosal, P. Haro-Gonzalez, A. Benayas, J. L. Plaza, E. Martín Rodríguez, J. García Solé, *Nanoscale* **2014**, *6*, 9494.
[25] Y. Ju, H. Zhang, J. Yu, S. Tong, N. Tian, Z. Wang, X. Wang, X. Su, X. Chu, J. Lin, Y. Ding, G. Li, F. Sheng, Y. Hou, *ACS Nano* **2017**, *11*, 9239.
[26] Q. Sun, Q. You, X. Pang, X. Tan, J. Wang, L. Liu, F. Guo, F. Tan, N. Li, *Biomaterials* **2017**, *122*, 188.
[27] A. M. Alkilany, L. B. Thompson, S. P. Boulos, P. N. Sisco, C. J. Murphy, *Adv. Drug Deliv. Rev.* **2012**, *64*, 190.

[28] X. Huang, S. Neretina, M. A. El-Sayed, *Adv. Mater.* **2009**, *21*, 4880.
[29] T. K. Sau, A. L. Rogach, F. Jäckel, T. A. Klar, J. Feldmann, *Adv. Mater.* **2010**, *22*, 1805.
[30] X. Ye, L. Jin, H. Caglayan, J. Chen, G. Xing, C. Zheng, V. Doan-Nguyen, Y. Kang, N. Engheta, C. R. Kagan, C. B. Murray, *ACS Nano* **2012**, *6*, 2804.
[31] X. Ye, C. Zheng, J. Chen, Y. Gao, C. B. Murray, *Nano Lett.* **2013**, *13*, 765.
[32] C. J. Murphy, L. B. Thompson, A. M. Alkilany, P. N. Sisco, S. P. Boulos, S. T. Sivapalan, J. A. Yang, D. J. Chernak, J. Huang, *J. Phys. Chem. Lett.* **2010**, *1*, 2867.
[33] N. N. Long, L. Van Vu, C. D. Kiem, S. C. Doanh, C. T. Nguyet, P. T. Hang, N. D. Thien, L. M. Quynh, *J. Phys. Conf. Ser.* **2009**, *187*, 12026.
[34] N. R. Jana, *Small* **2005**, *1*, 875.
[35] H. Chen, L. Shao, Q. Li, J. Wang, *Chem. Soc. Rev.* **2013**, *42*, 2679.
[36] B. Nikoobakht, M. A. El-Sayed, *Chem. Mater.* **2003**, *15*, 1957.
[37] R. N. Moussawi, D. Patra, *J. Phys. Chem. C* **2015**, *119*, 19458.
[38] S. W. Chu, H. Y. Wu, Y. T. Huang, T. Y. Su, H. Lee, Y. Yonemaru, M. Yamanaka, R. Oketani, S. Kawata, S. Shoji, K. Fujita, *ACS Photonics* **2014**, *1*, 32.
[39] H. I. Elim, J. Yang, J.-Y. Lee, J. Mi, W. Ji, *Appl. Phys. Lett.* **2006**, *88*, 83107.

Table 1. Synthetic parameters experimented and the resulting dimension, aspect ratio, and L-LSPR maximum wavelength of Au NRs.

Sample	4.15 mM $AgNO_3$ solution (mL)	Au seed solution (mL)	12.1 M HCl solution (mL)	NaOL (g)	NR average length (nm)[a)]	NR average diameter (nm)[a)]	Aspect ratio	L-LSPR maximum (nm)
a	24	0.3	2.1	1.234	107.2±7.9	24.0±2.2	4.47	903
b	36	0.2	2.1	1.234	103.1±9.0	22.2±1.9	4.65	943
c	24	0.2	2.1	1.234	103.3±6.5	19.9±1.1	5.19	966
d	24	0.3	2.1	1.234	95.9±16.2	17.5±3.7	5.48	980
e	24	0.4	2.1	1.234	81.7±5.7	14.1±1.6	5.81	1050
f	24	0.8	4.2	1.234	86.1±7.7	12.8±1.8	6.74	1143
g	24	0.8	4.2	0.925	132.3±16.9	17.5±2.0	7.57	1193
h	24	0.8	5.4	0.925	93.5±13.8	8.6±1.4	10.96	1300

[a)] Error bars are calculated based on the measurements of 50 Au NRs by TEM.

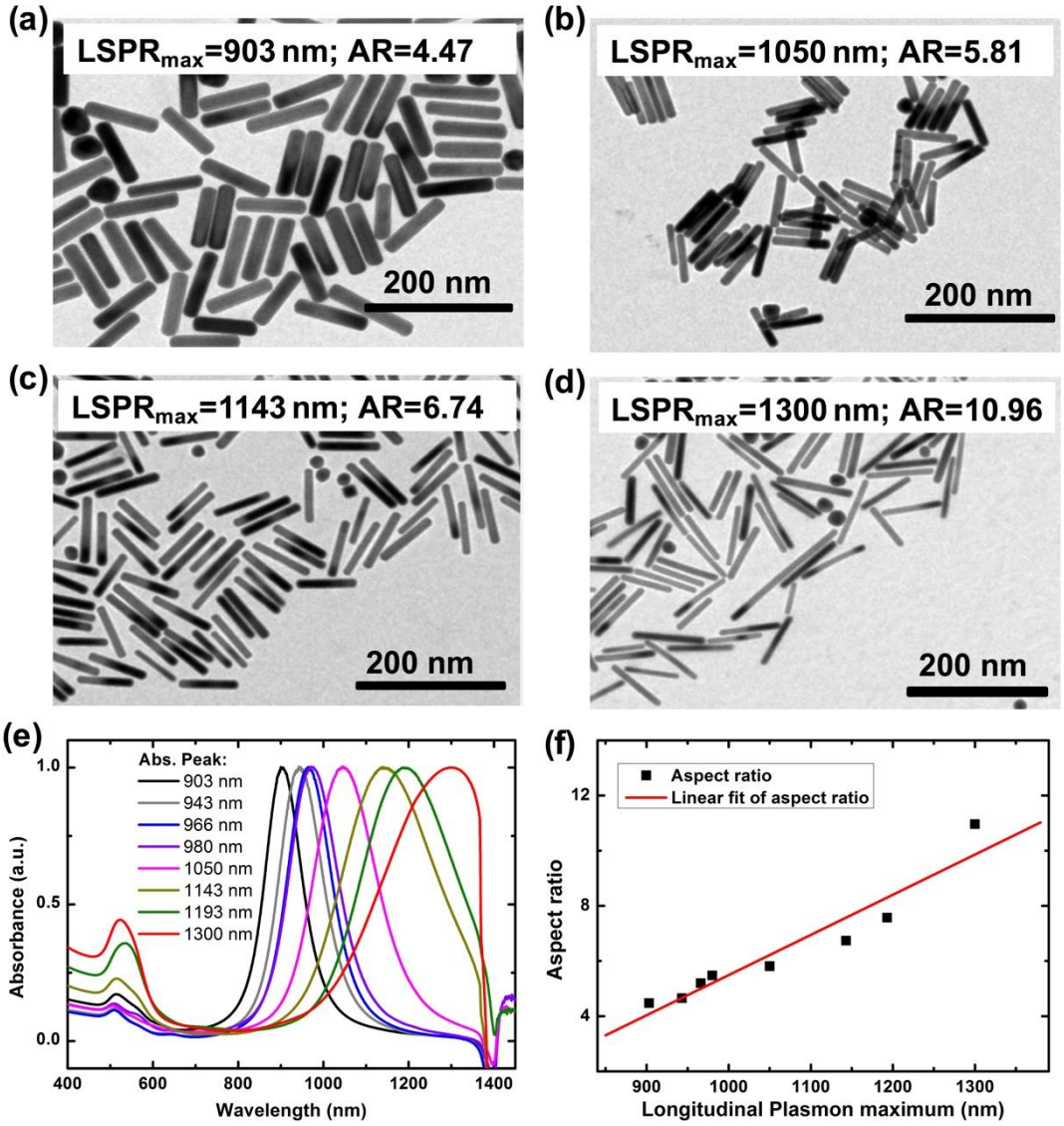

Figure 1. (a-d) TEM images of Au NRs with different aspect ratio (AR) and L-LSPR absorbance maximum. (a-d) correspond to the sample a, e, f and h listed in table 1 respectively. TEM images of other samples of table 1 are shown in the supporting information. (e) Absorbance spectrum of Au NRs in water. The absorbance feature at 1400 nm originates from the absorption of water. (f) The evolution of the L-LSPR maximum over the AR of Au NRs. Red curve represents the linear fit of the data.

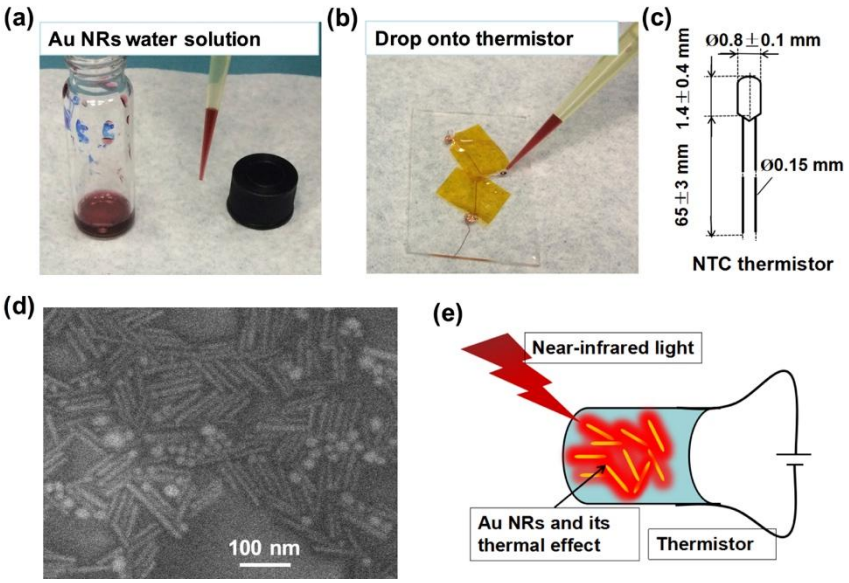

Figure 2. (a) Au NRs in water (sample h of table 1). (b) Image showing a NTC thermistor fixed on a glass slide. Au NR water solution was drop-casted onto the thermistor. (c) The dimension of the thermistor applied in this work. (d) SEM image of the Au NR-coated thermistor (with 3 μL of 1.2 g/L Au NR solution deposited on top) exhibiting mostly Au NRs on the surface of the hybrid device. (e) A schematic describing the hybrid Au-NR/thermistor device structure to harvest the photothermal effect of Au NRs for SWIR sensing.

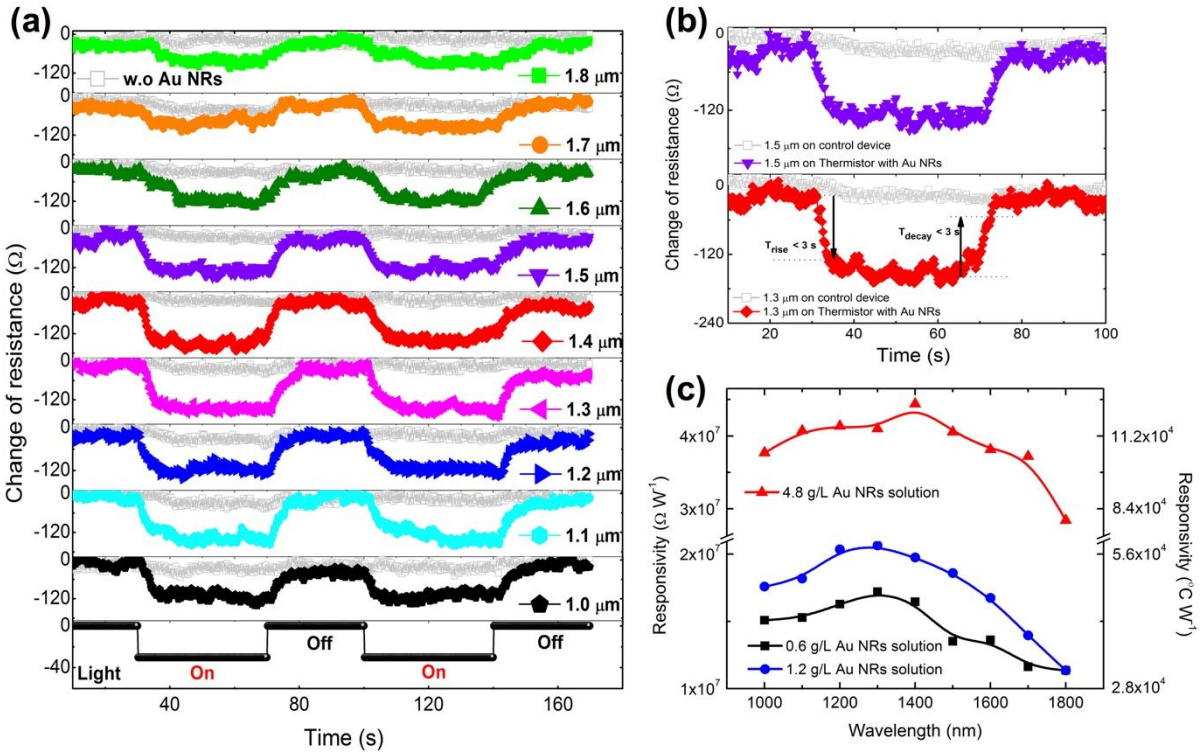

Figure 3. (a) Photoresponse characteristics over time of a hybrid Au-NR/thermistor device (fabricated by 4.8 g/L Au NR solution) in the form of photo-induced resistance drop upon exposure of monochromatic illumination (λ from 1.0 μm to 1.8 μm). Grey curves with open symbols represent the photoresponse from a control device without Au NRs. (b) Zoom-in view of the photoresponse characteristics in (a) under 1.4 μm and 1.5 μm illumination exhibiting the time scale of the response speed. Right-hand-side Y-axis represents the current measured under a DC bias of 1V. (c) The photoresponsivity (in Ω/W or in °C/W) of three batches of Au-NR/thermistor devices fabricated by different concentrations of Au NR solution over the whole wavelength window tested. All resistance was measured under a DC bias of 1 V at room-temperature.

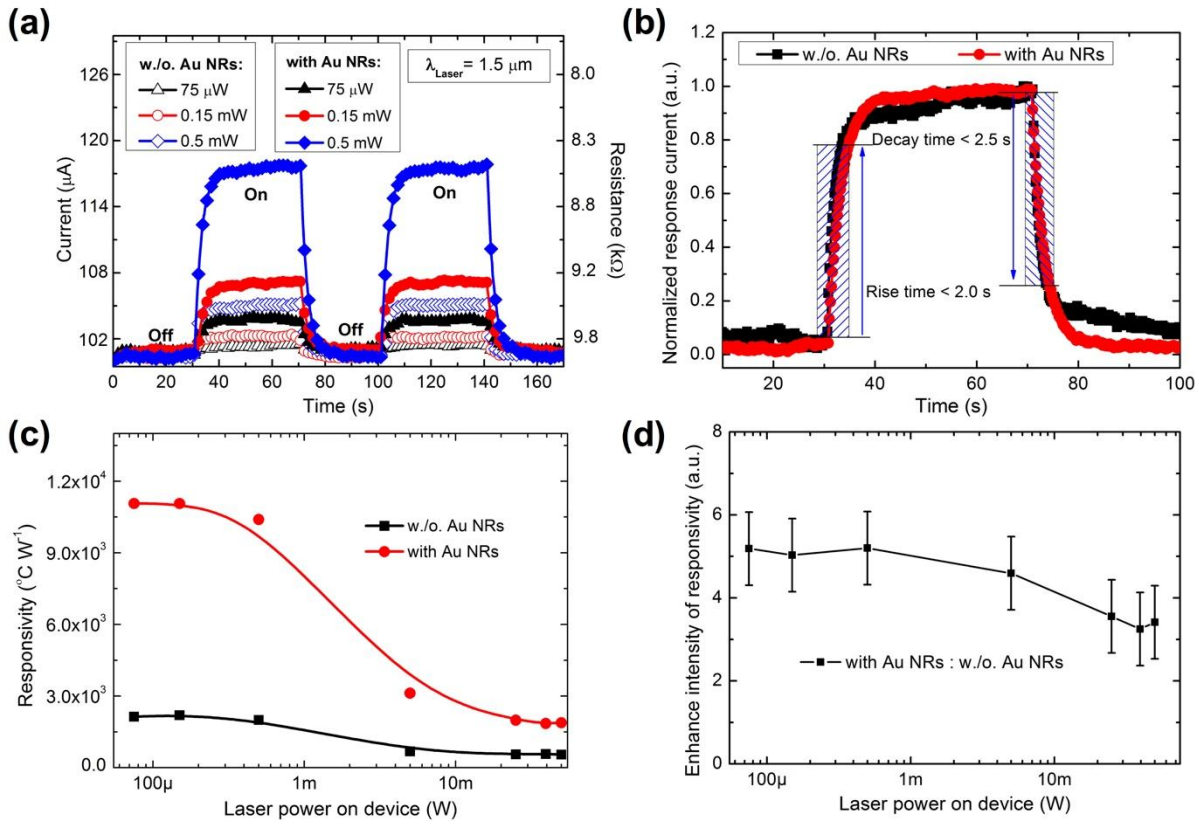

Figure 4. (a) Photoresponse characteristics over time of both the control device (thermistor without Au NRs) and the hybrid Au-NR/thermistor device (fabricated by 4.8 g/L Au NR solution) under the illumination of a laser (λ = 1.5 μm) focused on device. The photoresponse is presented in the form of photo-induced resistance drop (Ω, right Y axis) or in photo-induced change of measured current under a DC bias of 1V (Amperes, left Y axis). (b) Normalized of photoresponse characteristics (in measured current) comparing the control and the hybrid device under the illumination of a laser (λ = 1.5 μm, 0.5 mW, focused on device). Current was measured under a DC bias of 1V. (c) The evolution of the photoresponsivity (in °C/W) under the illumination of a laser (λ = 1.5 μm) of the control and the hybrid device over different laser powers experimented. (d) The enhancement ratios calculated from the photoresponsivity (shown in c) of the hybrid device over the control device (without Au NRs) at different laser powers.

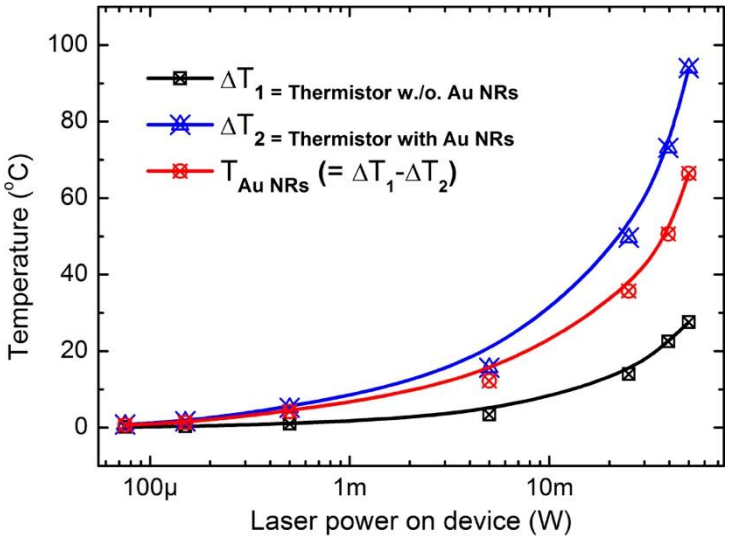

Figure 5. Evolution of the photo-induced temperature change over laser power of the control (black curve) and the optimized hybrid Au-NR/thermistor device fabricated by 4.8 g/L Au NR solution (blue curve) under the illumination of a laser (λ = 1.5 μm) which was focused on device. Red curve shows the contribution from Au NRs.